

# Normalized multi-pion Hanbury Brown-Twiss correlation functions of pion-emitting sources with Bose-Einstein condensation

Ghulam Bary, Peng Ru, Wei-Ning Zhang\*

*School of Physics, Dalian University of Technology, Dalian, Liaoning 116024, China*

## Abstract

Recently, the ALICE collaboration analyzed the three- and four-pion Hanbury Brown-Twiss (HBT) correlations in Pb-Pb collisions at the Large Hadron Collider (LHC). The measured suppressions of three- and four-pion correlations may originate from a substantial coherence of the particle-emitting sources. In this work we investigate the normalized three- and four-pion HBT correlation functions for evolving pion gas (EPG) sources with Bose-Einstein condensation. We find that the intercepts of the normalized correlation functions at zero relative momentum are sensitive to source condensation and particle momentum. The normalized correlation functions in low average-momentum regions of three and four pions decrease with decreasing temperature and increasing particle number of the source, indicating a dependence of the normalized correlation functions on source condensation. However, this dependence becomes weak in an intermediate average-momentum region because particles with high momenta are likely emitted from excited states incoherently in the EPG model, even if the source has a considerable condensation fraction. For a wide momentum range, the normalized correlation functions for low source temperatures are enhanced at larger relative momenta because of a rapid increase of two-pion chaoticity parameter with increasing particle momentum. We hope the significant enhancement of the normalized four-pion correlation function at high relative momentum will be identified through future analyses of experimental data.

Keywords: HBT interferometry, normalized multi-pion correlation functions, Bose-Einstein condensation, source coherence, ultra-relativistic heavy-ion collisions

PACS numbers: 25.75.Gz, 05.30.Jp

---

\* wnzhang@dlut.edu.cn

## I. INTRODUCTION

Two-pion Hanbury Brown-Twiss (HBT) interferometry is widely used to extract the space-time structure of pion-emitting sources produced in high-energy heavy-ion collisions [1–6]. One widely used parameter in analyses of two-pion HBT interferometry is the chaoticity parameter,  $\lambda$ , which is introduced by assuming a contribution of coherent particle emission. The chaoticity parameter is also related to many other effects in high-energy heavy-ion collisions, such as particle misidentification, final-state Coulomb interaction, long-lived resonance decay, pion laser emission, and so on [1–8].

As an extension of two-pion interferometry, multi-pion interferometry has been used in high-energy heavy-ion collisions [4, 5, 7–25]. The multi-pion correlation (MPC) analyses not only give an alternative way to test the physics obtained by two-pion interferometry, but also provide additional information of the particle-emitting sources. For example, the triplet identical pion correlation includes the phase of source function and its effect is important for asymmetric particle-emitting sources. More important, MPCs are more sensitive to the source coherence compared to two-pion correlation. In the heavy-ion collisions at the LHC energy, the identical pion multiplicity can reach several thousand. The high pion multiplicity and the technical development of MPC analysis [23] open the door to accurately measure the MPCs in experiment. Recently, the ALICE collaboration at the LHC find that there is a significant suppression of MPCs in Pb-Pb collisions, and this suppression does not be observed in the  $pp$  and  $p$ -Pb collisions [24]. It may indicate that the suppression is a kind of medium effect of many particles.

In our previous work [25], we investigated the three- and four-pion HBT correlation functions for heavy-ion collisions at the LHC [24], based on an evolving pion gas (EPG) model with Bose-Einstein condensation [26]. Our model results of MPC functions were consistent with experimental data and indicated a source condensation fraction between 16% and 47% [25]. Pion condensation may also enhance the pion-transverse-momentum spectrum in low transverse-momentum region in heavy-ion collisions at the LHC [27]. However, to determine the source condensation fraction with the HBT technique, one has to remove the other effects on chaoticity parameters, especially the effect of long-lived resonance decay.

In Ref. [15], Heinz, Zhang, and Sugarbaker proposed the normalized three-pion correlation function  $r_3$ , which can be used to determine the degree of source coherence without

contamination from resonance decays. The function  $r_3$  has been used to analyze experimental data for heavy-ion collisions at the CERN-SPS [17, 18], RHIC [19], and LHC [22]. In this article, we investigate the normalized three-pion and four-pion correlation functions,  $r_3$  and  $r_4$ , in the EPG model for heavy-ion collisions at the LHC. The results show that the normalized MPC functions in low average-transverse-momentum region are sensitive to EPG source condensation. The increase of the normalized MPC functions at high relative momenta reflects the particle-correlation characteristic in the EPG model, that the correlations decrease rapidly with increasing particle momentum.

This article consists of four sections. We present some basic MPC formulas and study the intercepts of normalized MPC functions in the EPG model in section 2. In section 3, we show and discuss the results of the normalized three- and four-pion correlation functions in the EPG model. Finally, we give a summary and discussions in section 4.

## II. INTERCEPTS OF NORMALIZED MPC FUNCTIONS IN THE EPG MODEL

By the definitions of HBT correlation functions with density matrices, the two-, three-, and four-pion correlation functions can be written as [25]

$$C_2(\mathbf{p}_1, \mathbf{p}_2) = 1 + R_2(\mathbf{p}_1, \mathbf{p}_2), \quad (1)$$

$$C_3(\mathbf{p}_1, \mathbf{p}_2, \mathbf{p}_3) = 1 + R_2(\mathbf{p}_1, \mathbf{p}_2) + R_2(\mathbf{p}_1, \mathbf{p}_3) + R_2(\mathbf{p}_2, \mathbf{p}_3) + R_3(\mathbf{p}_1, \mathbf{p}_2, \mathbf{p}_3), \quad (2)$$

$$\begin{aligned} C_4(\mathbf{p}_1, \mathbf{p}_2, \mathbf{p}_3, \mathbf{p}_4) = & 1 + R_2(\mathbf{p}_1, \mathbf{p}_2) + R_2(\mathbf{p}_1, \mathbf{p}_3) + R_2(\mathbf{p}_1, \mathbf{p}_4) + R_2(\mathbf{p}_2, \mathbf{p}_3) \\ & + R_2(\mathbf{p}_2, \mathbf{p}_4) + R_2(\mathbf{p}_3, \mathbf{p}_4) + R_3(\mathbf{p}_1, \mathbf{p}_2, \mathbf{p}_3) + R_3(\mathbf{p}_1, \mathbf{p}_2, \mathbf{p}_4) \\ & + R_3(\mathbf{p}_1, \mathbf{p}_3, \mathbf{p}_4) + R_3(\mathbf{p}_2, \mathbf{p}_3, \mathbf{p}_4) + R_2(\mathbf{p}_1, \mathbf{p}_2)R_2(\mathbf{p}_3, \mathbf{p}_4) \\ & + R_2(\mathbf{p}_1, \mathbf{p}_3)R_2(\mathbf{p}_2, \mathbf{p}_4) + R_2(\mathbf{p}_1, \mathbf{p}_4)R_2(\mathbf{p}_2, \mathbf{p}_3) \\ & + R_4(\mathbf{p}_1, \mathbf{p}_2, \mathbf{p}_3, \mathbf{p}_4) + R_4(\mathbf{p}_1, \mathbf{p}_2, \mathbf{p}_4, \mathbf{p}_3) + R_4(\mathbf{p}_1, \mathbf{p}_3, \mathbf{p}_2, \mathbf{p}_4). \end{aligned} \quad (3)$$

Here,  $R_2(\mathbf{p}_i, \mathbf{p}_j)$ ,  $[R_2(\mathbf{p}_i, \mathbf{p}_j)R_2(\mathbf{p}_k, \mathbf{p}_l)]$ ,  $R_3(\mathbf{p}_i, \mathbf{p}_j, \mathbf{p}_k)$ , and  $R_4(\mathbf{p}_i, \mathbf{p}_j, \mathbf{p}_k, \mathbf{p}_l)$  denote the correlation of a single pion pair, correlation of a double pion pair, pure pion-triplet interference or true three-pion correlator [9, 15], and pure pion-quadruplet interference, respectively.

The particle-emitting source in the EPG model [26] is a quasi-static identical-pion gas trapped within a mean field with harmonic oscillator potential [28]  $\sim (\hbar\omega r^2/a^2)$ , where

$a = \sqrt{\hbar/m\omega}$  is the characteristic length of the harmonic oscillator. The harmonic oscillator potential has been used to study Bose-Einstein condensation in atomic physics [29–31]. Its advantage here is that the pion gas system can be analytically solved in nonrelativistic cases [28], although the particle motion is relativistic in our model calculations [25, 26]. In the EPG model, the source evolution is assumed to be an adiabatic expansion satisfying  $TV^{\gamma-1} = \text{constant}$  at each state of evolution, which is an approximation for the case that the system relaxation time is shorter than the source evolution time. Here,  $T$  is the temperature and  $V$  is the volume of the source. For a source expanding spherically, it is assumed that  $a = C_1 R = C_1(R_0 + \alpha t)$  [26], where  $C_1$  is the source-size parameter,  $R_0$  is the initial source radius, and  $\alpha$  is a parameter related to the average expansion velocity of the source. With a hydrodynamical calculation for  $R_0 = 6$  fm and  $T_0 = 170$  MeV, the model parameters  $\gamma$  and  $\alpha$  are fixed at 1.627 and 0.62 [26], respectively. In the model calculations of this paper, the values of  $C_1$  are taken to be 0.35 and 0.40 as in Refs. [25, 26].

For the EPG source with Bose-Einstein condensation, the functions are [25]

$$R_2(\mathbf{p}_i, \mathbf{p}_j) = \frac{|G^{(1)}(\mathbf{p}_i, \mathbf{p}_j)|^2 - N_0^2 |u_0(\mathbf{p}_i)|^2 |u_0(\mathbf{p}_j)|^2}{G^{(1)}(\mathbf{p}_i, \mathbf{p}_i) G^{(1)}(\mathbf{p}_j, \mathbf{p}_j)}, \quad (4)$$

$$R_3(\mathbf{p}_i, \mathbf{p}_j, \mathbf{p}_k) = \frac{2 \operatorname{Re} [G^{(1)}(\mathbf{p}_i, \mathbf{p}_j) G^{(1)}(\mathbf{p}_j, \mathbf{p}_k) G^{(1)}(\mathbf{p}_k, \mathbf{p}_i) - N_0^3 f_3(\mathbf{p}_i, \mathbf{p}_j, \mathbf{p}_k)]}{G^{(1)}(\mathbf{p}_i, \mathbf{p}_i) G^{(1)}(\mathbf{p}_j, \mathbf{p}_j) G^{(1)}(\mathbf{p}_k, \mathbf{p}_k)}, \quad (5)$$

and

$$R_4(\mathbf{p}_i, \mathbf{p}_j, \mathbf{p}_k, \mathbf{p}_l) = \frac{2 \operatorname{Re} [G^{(1)}(\mathbf{p}_i, \mathbf{p}_j) G^{(1)}(\mathbf{p}_j, \mathbf{p}_k) G^{(1)}(\mathbf{p}_k, \mathbf{p}_l) G^{(1)}(\mathbf{p}_l, \mathbf{p}_i) - N_0^4 f_4(\mathbf{p}_i, \mathbf{p}_j, \mathbf{p}_k, \mathbf{p}_l)]}{G^{(1)}(\mathbf{p}_i, \mathbf{p}_i) G^{(1)}(\mathbf{p}_j, \mathbf{p}_j) G^{(1)}(\mathbf{p}_k, \mathbf{p}_k) G^{(1)}(\mathbf{p}_l, \mathbf{p}_l)}, \quad (6)$$

where  $G^{(1)}(\mathbf{p}_i, \mathbf{p}_j)$  is the one-particle density matrix,  $N_0$  is the ground-state particle number, and  $u_n(\mathbf{p})$  ( $n = 0, 1, 2, \dots$ ) is the single-particle wave function, and

$$G^{(1)}(\mathbf{p}_i, \mathbf{p}_j) = \sum_n u_n^*(\mathbf{p}_i) u_n(\mathbf{p}_j) \frac{g_n \mathcal{Z} e^{-\tilde{E}_n/T}}{1 - \mathcal{Z} e^{-\tilde{E}_n/T}}, \quad (7)$$

where  $g_n$  is the degeneracy,  $\mathcal{Z}$  is the fugacity parameter including the factor for the lowest energy level  $\varepsilon_0$ , and  $\tilde{E}_n$  is the eigenenergy of a relativistic pion relative to  $\varepsilon_0$  [25, 26, 28, 30]. In Eqs. (5) and (6),  $f_3(\mathbf{p}_i, \mathbf{p}_j, \mathbf{p}_k)$  and  $f_4(\mathbf{p}_i, \mathbf{p}_j, \mathbf{p}_k, \mathbf{p}_l)$  are functions of  $u_0(\mathbf{p})$ ,  $G^{(1)}(\mathbf{p}_i, \mathbf{p}_j)$ ,

and  $N_0$  [25]. For a completely chaotic source,  $N_0 \ll N$ , the second terms in the numerators in Eqs. (4), (5), and (6) approach 0. However, in the nearly completely coherent case, almost all particles are in the ground condensate state, functions  $f_3(\mathbf{p}_i, \mathbf{p}_j, \mathbf{p}_k) \rightarrow |u_0(\mathbf{p}_i)|^2 |u_0(\mathbf{p}_j)|^2 |u_0(\mathbf{p}_k)|^2$  and  $f_4(\mathbf{p}_i, \mathbf{p}_j, \mathbf{p}_k, \mathbf{p}_l) \rightarrow |u_0(\mathbf{p}_i)|^2 |u_0(\mathbf{p}_j)|^2 |u_0(\mathbf{p}_k)|^2 |u_0(\mathbf{p}_l)|^2$ , and the two terms in the numerators in Eqs. (4), (5), and (6) approximately cancel each other. Therefore, the two-pion, three-pion, and four-pion correlation functions approach 1 in the completely coherent case [26]. From Eq. (7), we can calculate the density matrices  $G^{(1)}(\mathbf{p}_i, \mathbf{p}_j)$  for the EPG source at each evolution step (with given temperature  $T$  and total particle number  $N$ ) with the technique developed in Ref. [28], and then obtain the two-, three-, and four-pion correlation functions [25, 26, 28].

The normalized three-pion correlation function  $r_3(\mathbf{p}_1, \mathbf{p}_2, \mathbf{p}_3)$  is defined by dividing  $R_3(\mathbf{p}_1, \mathbf{p}_2, \mathbf{p}_3)$  by the square root of the product of the two-particle correlators [15]:

$$r_3(\mathbf{p}_1, \mathbf{p}_2, \mathbf{p}_3) = \frac{R_3(\mathbf{p}_1, \mathbf{p}_2, \mathbf{p}_3)}{\sqrt{R_2(\mathbf{p}_1, \mathbf{p}_2)R_2(\mathbf{p}_2, \mathbf{p}_3)R_2(\mathbf{p}_3, \mathbf{p}_1)}}. \quad (8)$$

Function  $r_3$  is insensitive to resonance decay [15, 17–19, 22], and is directly related to the condensation fraction for our space-symmetric EPG sources. Similarly, the normalized four-pion correlation function  $r_4(\mathbf{p}_1, \mathbf{p}_2, \mathbf{p}_3, \mathbf{p}_4)$  is defined by [23]

$$r_4(\mathbf{p}_1, \mathbf{p}_2, \mathbf{p}_3, \mathbf{p}_4) = \frac{R_{44}(\mathbf{p}_1, \mathbf{p}_2, \mathbf{p}_3, \mathbf{p}_4)}{\sqrt{R_2(\mathbf{p}_1, \mathbf{p}_2)R_2(\mathbf{p}_2, \mathbf{p}_3)R_2(\mathbf{p}_3, \mathbf{p}_4)R_2(\mathbf{p}_4, \mathbf{p}_1)}}, \quad (9)$$

where

$$R_{44}(\mathbf{p}_1, \mathbf{p}_2, \mathbf{p}_3, \mathbf{p}_4) = R_4(\mathbf{p}_1, \mathbf{p}_2, \mathbf{p}_3, \mathbf{p}_4) + R_4(\mathbf{p}_1, \mathbf{p}_2, \mathbf{p}_4, \mathbf{p}_3) + R_4(\mathbf{p}_1, \mathbf{p}_3, \mathbf{p}_2, \mathbf{p}_4). \quad (10)$$

In the EPG model, the intercept of  $R_2(\mathbf{p}_1, \mathbf{p}_2)$  at zero relative momentum can be written as [26]

$$\lambda(\mathbf{p}) = R_2(\mathbf{p}, \mathbf{p}) = 1 - \frac{N_0^2 |u_0(\mathbf{p})|^4}{G^{(1)}(\mathbf{p}, \mathbf{p})^2} \equiv 1 - [f_0 F_N(\mathbf{p})]^2, \quad (11)$$

where  $f_0 = N_0/N$  is the condensation fraction and

$$F_N(\mathbf{p}) = N |u_0(\mathbf{p})|^2 / G^{(1)}(\mathbf{p}, \mathbf{p}). \quad (12)$$

Hence, the intercepts of  $r_3$  and  $r_4$  at zero relative momentum  $q_{ij} = \sqrt{-(p_i - p_j)^\mu (p_i - p_j)_\mu} = 0$ , ( $i, j = 1, 2, 3, 4$ ) can be written as

$$I_3(\mathbf{p}) \equiv r_3(\mathbf{p}, \mathbf{p}, \mathbf{p}) = 2 \frac{1 - 3[f_0 F_N(\mathbf{p})]^2 + 2[f_0 F_N(\mathbf{p})]^3}{[1 - [f_0 F_N(\mathbf{p})]^2]^{3/2}} \quad (13)$$

and

$$I_4(\mathbf{p}) \equiv r_4(\mathbf{p}, \mathbf{p}, \mathbf{p}, \mathbf{p}) = 6 \frac{1 - 6[f_0 F_N(\mathbf{p})]^2 + 8[f_0 F_N(\mathbf{p})]^3 - 3[f_0 F_N(\mathbf{p})]^4}{[1 - [f_0 F_N(\mathbf{p})]^2]^2}. \quad (14)$$

These intercepts are functions of condensation fraction  $f_0$  and particle momentum  $\mathbf{p}$ , and thus are functions of system temperature  $T$ , particle number  $N$ , source-size parameter  $C_1$  [25, 26], and particle momentum  $\mathbf{p}$ .

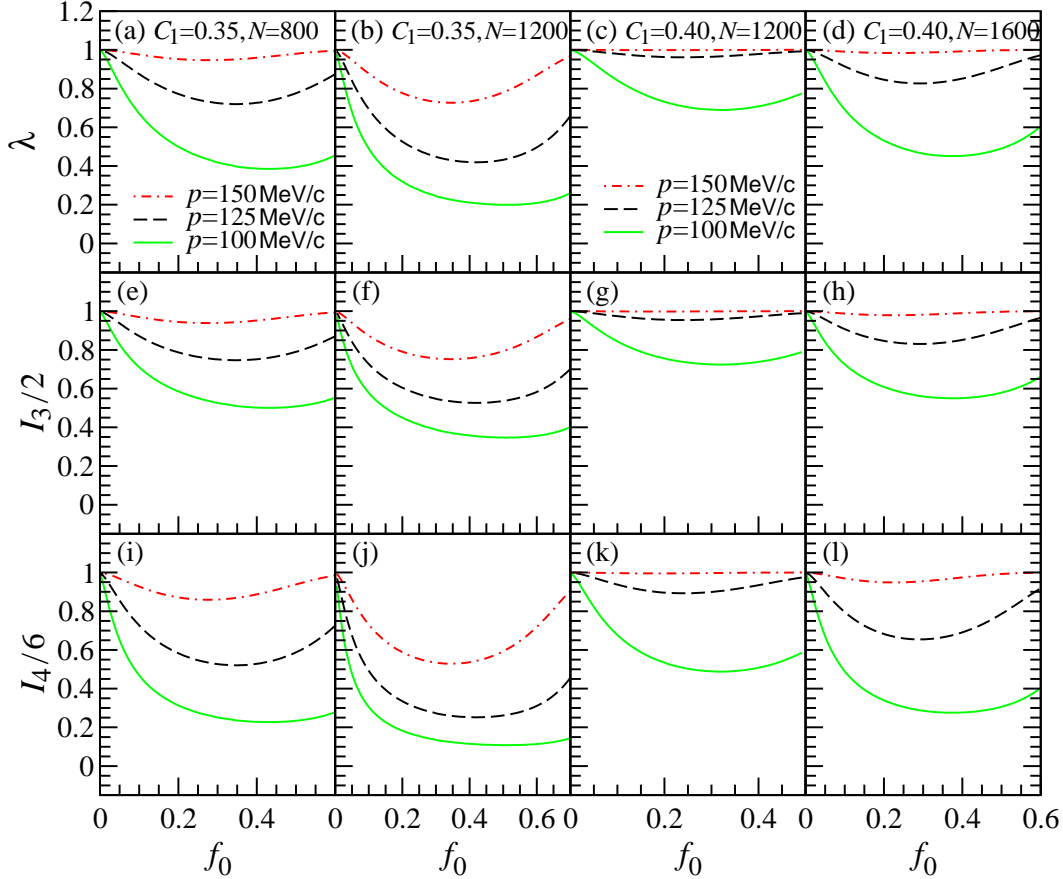


FIG. 1: (Color online) Intercepts of two-pion correlation function,  $\lambda$ , and of normalized three- and four-pion correlation functions,  $I_3$  and  $I_4$ , as functions of condensation fraction  $f_0$  for EPG sources with different values of source-size parameter  $C_1$ , particle number  $N$ , and particle momentum  $p$ .

We plot in Figs. 1(a)–(d), 1(e)–(h), and 1(i)–(l) the intercepts  $\lambda$ ,  $I_3$ , and  $I_4$ , respectively, as functions of the condensation fraction  $f_0$  for EPG sources with different values of source-size parameter  $C_1$ , particle number  $N$ , and particle momentum  $p = |\mathbf{p}|$ . The variational tendencies of  $\lambda(f_0)$ ,  $I_3(f_0)/2$ , and  $I_4(f_0)/6$  are almost the same. They are 1 when  $f_0 = 0$ . As  $f_0$  increases from 0, the intercepts decrease to their minima, and then increase with increasing  $f_0$ . The decreases of the intercepts are much smaller for higher momentum. This

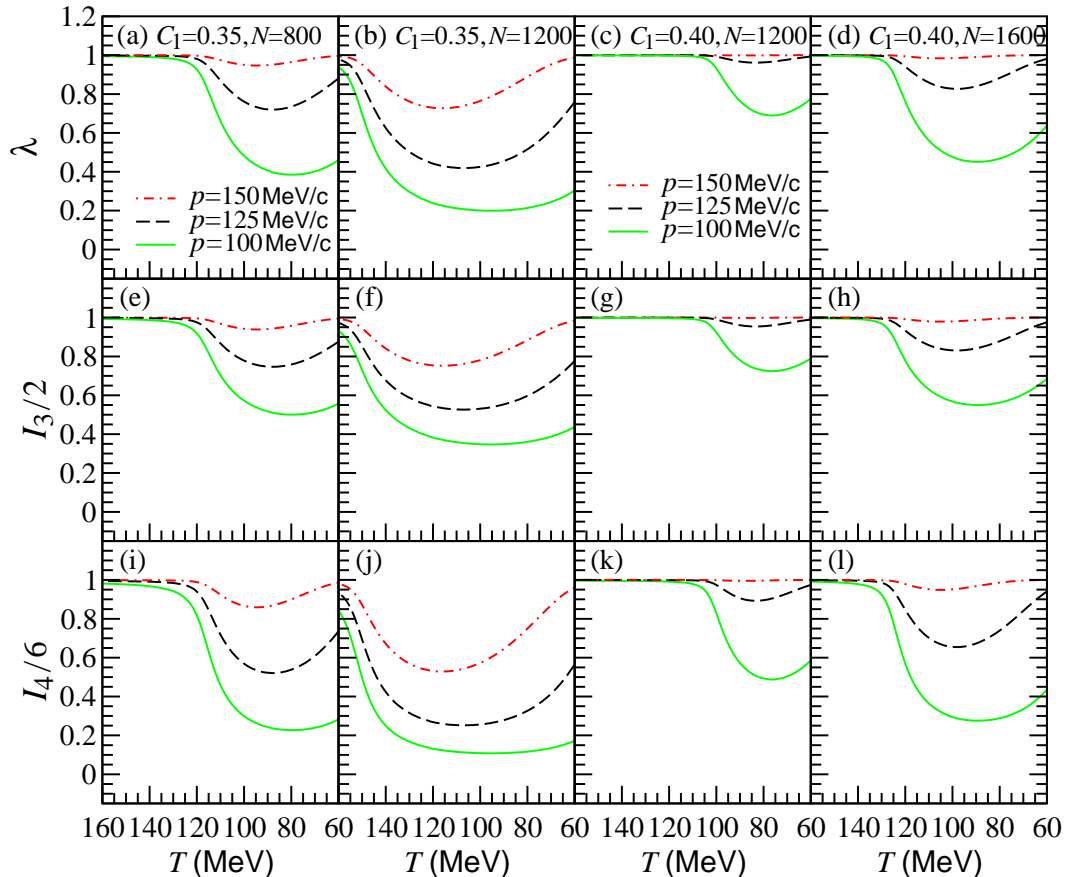


FIG. 2: (Color online) Intercepts of two-pion correlation function,  $\lambda$ , and of normalized three- and four-pion correlation functions,  $I_3$  and  $I_4$ , as functions of temperature  $T$  for EPG sources with different values of source-size parameter  $C_1$ , particle number  $N$ , and particle momentum  $p$ .

is because the particles with higher momenta are likely emitted from the excited states incoherently, even from a source with finite  $f_0$ . For the same  $f_0$  value, the intercepts are smaller for the higher particle numbers and the smaller source-size parameter. This is due to the function  $F_N$  defined in Eq. (12), which increases with decreasing  $N$  and increasing  $C_1$  at low momentum in the EPG model (see Fig. 7 in Ref. [26]). From Eq. (11) we see that the intercept increases with increasing  $f_0$  if  $F_N(p)$  decreases more rapidly with increasing  $f_0$ . This is the reason for the increases of the intercepts for higher momentum at high  $f_0$  (with low source temperature).

We further plot in Figs. 2(a)–(d), 2(e)–(h), and 2(i)–(l) the intercepts  $\lambda$ ,  $I_3$ , and  $I_4$ , respectively, as functions of the source temperature  $T$  for EPG sources with different values of  $C_1$ ,  $N$ ,  $p$ . Because  $T$  and  $f_0$  have an antilinear relationship (see Fig. 19 in Ref. [25]), the

intercepts  $\lambda(T)$ ,  $I_3(T)/2$ , and  $I_4(T)/6$  have similar variations with decreasing  $T$  to those in Fig. 1 with increasing  $f_0$ . They are 1 at high temperature and decrease to their minima at low temperature. The minima decrease with decreasing  $p$ , increasing  $N$ , and decreasing  $C_1$ .

### III. RESULTS OF NORMALIZED MPC FUNCTIONS

In this section we analyze the normalized MPC functions  $r_3(Q_3)$  and  $r_4(Q_4)$  in different regions of the average transverse momenta  $K_{T3}$  and  $K_{T4}$  in the EPG model, and compare the model results with corresponding experimental data [22]. Here,

$$Q_3 = \sqrt{q_{12}^2 + q_{13}^2 + q_{23}^2}, \quad (15)$$

$$Q_4 = \sqrt{q_{12}^2 + q_{13}^2 + q_{14}^2 + q_{23}^2 + q_{24}^2 + q_{34}^2}, \quad (16)$$

$$K_{T3} = \frac{|\mathbf{p}_{1T} + \mathbf{p}_{2T} + \mathbf{p}_{3T}|}{3}, \quad (17)$$

$$K_{T4} = \frac{|\mathbf{p}_{1T} + \mathbf{p}_{2T} + \mathbf{p}_{3T} + \mathbf{p}_{4T}|}{4}. \quad (18)$$

#### A. Results for $r_3(Q_3)$

We plot in Fig. 3 the normalized three-pion correlation function  $r_3(Q_3)$  for different source temperatures and small and large particle numbers,  $N = 400$  and  $800$ , in the EPG model with  $C_1 = 0.35$ . In the low average-transverse-momentum region  $0 < K_{T3} < 0.16$  GeV/ $c$ ,  $r_3(Q_3)$  decreases with decreasing  $T$  and is lower for high  $N$ . This is because the system has more condensation at lower temperature and higher particle number than at higher temperature and lower particle number. For the low particle number,  $r_3(Q_3)$  decreases with increasing  $Q_3$ . However, for high particle number and low temperature,  $T = 80$  MeV,  $r_3(Q_3)$  increases slightly with increasing  $Q_3$ . In the intermediate average-transverse-momentum region  $0.16 < K_{T3} < 0.3$  GeV/ $c$ ,  $r_3(Q_3)$  results are higher than those in the low average-transverse-momentum region, and the dependences of  $r_3(Q_3)$  on the source temperature and particle number become weaker than those in the low average-transverse-momentum region. These reflect the important characteristic of the EPG source that the particles with high momenta are likely emitted from excited states thermally and incoherently even for the source with a considerable condensation fraction. In the high average-transverse-momentum



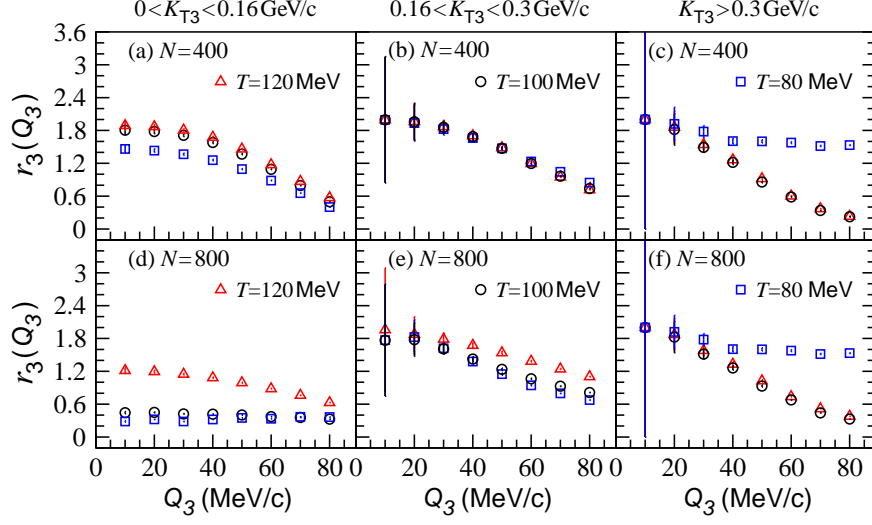


FIG. 3: (Color online) Normalized three-pion correlation function  $r_3(Q_3)$  for the EPG sources with different temperatures and particle numbers and in the transverse-momentum regions  $0 < K_{T3} < 0.16$  GeV/c,  $0.16 < K_{T3} < 0.3$  GeV/c, and  $K_{T3} > 0.3$  GeV/c. Here, the source-size parameter is  $C_1 = 0.35$ .

region  $K_{T3} > 0.3$  GeV/c,  $r_3(Q_3)$  is almost the same for the temperatures  $T = 120$  and  $100$  MeV. However,  $r_3(Q_3)$  becomes flat at large  $Q_3$  for the low temperature  $T = 80$  MeV.

To explain the variational tendency of  $r_3(Q_3)$  with increasing  $Q_3$ , we consider the special case  $\mathbf{p}_1 = \mathbf{p}_2$  in Eq. (8) for simplicity. In this case, we have

$$\begin{aligned}
 r_3(Q_3) &= \frac{2}{\sqrt{\lambda(p_2)}} \left[ 1 - \frac{2[1 - \lambda(p_2)]^{3/4}[1 - \lambda(p_3)]^{1/4}}{\sqrt{R_2^{ch}(q_{23})} + [1 - \lambda(p_2)]^{1/4}[1 - \lambda(p_3)]^{1/4}} \right] \\
 &\approx \frac{2}{\sqrt{\lambda(\bar{p})}} \left[ 1 - \frac{2[1 - \lambda(\bar{p})]}{\sqrt{R_2^{ch}(q_{23})} + \sqrt{1 - \lambda(\bar{p})}} \right] \\
 &= \frac{2}{\sqrt{\lambda(\bar{p})}} \left[ 1 - \frac{2\sqrt{1 - \lambda(\bar{p})}}{\sqrt{R_2^{ch}(q_{23})/\sqrt{1 - \lambda(\bar{p})} + 1}} \right], \quad (Q_3 = \sqrt{2}q_{23}), \quad (19)
 \end{aligned}$$

where  $0 < R_2^{ch}(q_{23}) < 1$  is the two-pion correlator of completely chaotic source, and  $\lambda(\bar{p})$  is the chaoticity parameter (intercept) of the two-pion correlation at average particle momentum  $\bar{p}$ . For a completely chaotic source,  $f_0 = 0$ ,  $\lambda(\bar{p}) = 1$ , and  $r_3(Q_3) = 2$ . For finite  $f_0$  and fixed  $\lambda(\bar{p})$ ,  $r_3(Q_3)$  decreases with increasing  $Q_3$  because  $R_2^{ch}(q_{23})$ , as a function of source size and  $Q_3$ , decreases with increasing  $Q_3$ . In fact, the value of  $\lambda$  in Eq. (19) is  $Q_3$ -dependent because  $\bar{p}$  is related to  $Q_3$ . The average particle momentum  $\bar{p}$  will increase with increasing  $Q_3$  if there are no other constraints. This leads to an increasing  $\lambda(\bar{p})$  (see Fig. 1) and de-

creasing  $[1 - \lambda(\bar{p})]$  with increasing  $Q_3$ . From Eq. (19) we see that  $r_3(Q_3)$  will increase with increasing  $Q_3$  if  $[1 - \lambda(\bar{p})]$  decreases with increasing  $Q_3$  faster than  $R_2^{ch}(q_{23})$  does. This may occur at low temperature, where  $\lambda(\bar{p})$  decreases rapidly with increasing particle momentum (see Fig. 2).

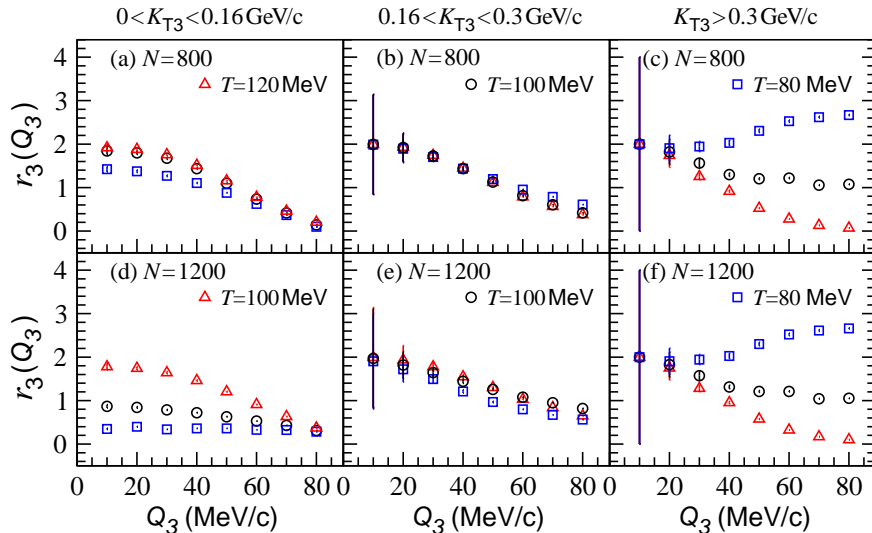


FIG. 4: (Color online) Normalized three-pion correlation function  $r_3(Q_3)$  for the EPG sources with different temperatures and particle numbers and in the transverse-momentum regions  $0 < K_{T3} < 0.16$  GeV/c,  $0.16 < K_{T3} < 0.3$  GeV/c, and  $K_{T3} > 0.3$  GeV/c. Here, the source-size parameter is  $C_1 = 0.40$ .

We plot in Fig. 4 the normalized three-pion correlation function  $r_3(Q_3)$  for EPG sources with  $C_1 = 0.40$  and  $N = 800$  and  $1200$ . The behaviors of  $r_3(Q_3)$  in the low and intermediate average-transverse-momentum regions are similar to those in Fig. 3. In the high average-transverse-momentum region, the results of  $r_3(Q_3)$  for the low temperatures obviously increase with increasing  $Q_3$  at large  $Q_3$  compared to the results for the high temperature. This is related to the increase of  $\lambda$  with increasing particle momentum in the wide momentum variational region.

We plot in Fig. 5 the normalized three-pion correlation function  $r_3(Q_3)$  for EPG sources in the average-transverse-momentum regions  $0 < K_{T3} < 0.16$  GeV/c,  $0.16 < K_{T3} < 0.3$  GeV/c, and  $0.3 < K_{T3} < 1$  GeV/c. Here, the values of temperature  $T$  and particle number  $N$  for the source with parameters  $C_1 = 0.35$  and  $0.40$  are taken as the same in Ref. [25] where the model results of MPCs  $C_3(Q_3)$ ,  $c_3(Q_3)$ ,  $C_4(Q_4)$ ,  $a_4(Q_4)$ ,  $b_4(Q_4)$ , and  $c_4(Q_4)$  are compared with the

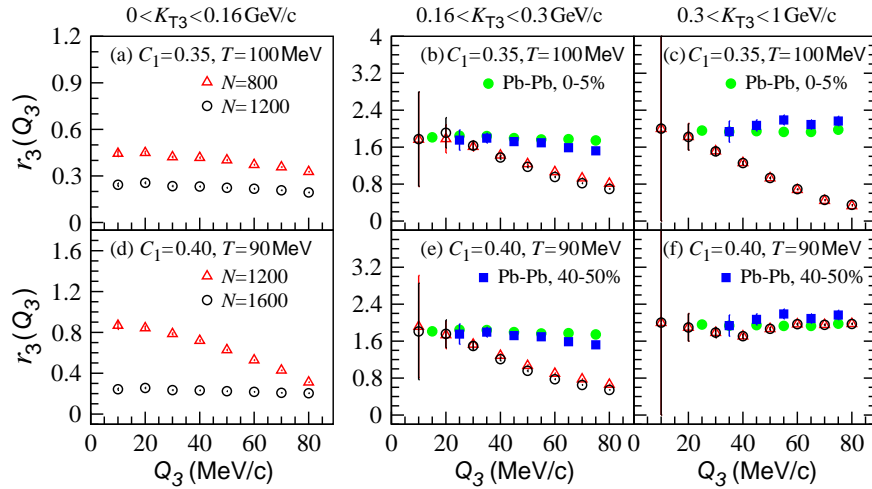


FIG. 5: (Color online) Top panels: Normalized three-pion correlation function  $r_3(Q_3)$  for the EPG sources with  $C_1 = 0.35$ ,  $T = 100$  MeV, and  $N = 800$  and  $1200$ . Bottom panels: Normalized three-pion correlation function  $r_3(Q_3)$  for the EPG sources with  $C_1 = 0.40$ ,  $T = 90$  MeV, and  $N = 1200$  and  $1600$ . The solid circle and square symbols in the middle and right panels are for the data in the central (0-5%) and peripheral (40-50%) Pb-Pb collisions at the LHC [22].

experimental data in the average-transverse-momentum regions  $0.16 < K_{T3} < 0.3$  GeV/ $c$  and  $0.3 < K_{T3} < 1$  GeV/ $c$  [24]. In the low transverse-momentum region (Figs. 5(a) and (d)), the results for the higher particle numbers are lower than those for the lower particle numbers because of severe condensation for the sources with higher  $N$ . However, in the intermediate and high transverse-momentum regions, the differences of  $r_3(Q_3)$  results for the lower and higher  $N$  values are small (see Figs. 5(b) and (e)) and the results are almost the same (see Figs. 5(c) and (f)). This is because the particles with high momenta are likely emitted from the excited states incoherently. In Fig. 5(b), (c), (e), and (f), the solid circles and squares denote the experimental  $r_3$  data for central and peripheral Pb-Pb collisions, respectively, at the LHC [22]. The experimental results are almost independent of collision centrality and almost flat with increasing  $Q_3$ . At small  $Q_3$ , the results of the EPG model agree with the experimental data. Furthermore, the model results in Fig. 5(f) almost reproduce the experimental data in the high transverse-momentum region. As discussed above, the variational tendency of  $r_3(Q_3)$  is related to the source size and  $\lambda$  increase with particle momentum. Because the EPG model considers only a simple source expanding spherically, it is unpractical to hope the model results can completely reproduce the experimental data.

## B. $r_4(Q_4)$ results

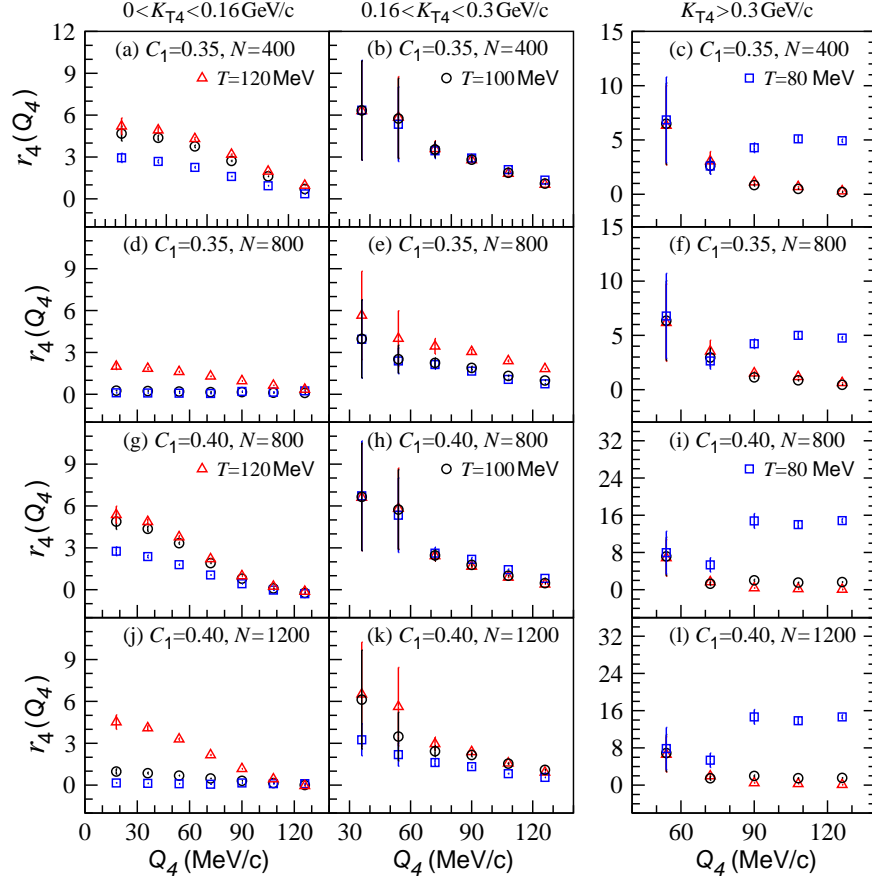


FIG. 6: (Color online) Normalized four-pion correlation functions  $r_4(Q_4)$  for the EPG sources with different source temperatures and particle numbers, and in the transverse-momentum intervals  $0 < K_{T4} < 0.16$  GeV/c,  $0.16 < K_{T4} < 0.3$  GeV/c, and  $K_{T4} > 0.3$  GeV/c. The source-size parameters  $C_1$  are 0.35 (the first and second rows) and 0.40 (the third and fourth rows).

We plot in Fig. 6 the normalized four-pion correlation function  $r_4(Q_4)$  for EPG sources with different temperatures and particle numbers as in Figs. 3 and 4. The variation of  $r_4(Q_4)$  as a function of  $Q_4$  is similar to that of  $r_3(Q_3)$  as a function of  $Q_3$ . In the low average-transverse-momentum region  $0 < K_{T4} < 0.16$  GeV/c,  $r_4(Q_4)$  decreases with decreasing temperature. In the intermediate average-transverse-momentum region  $0.16 < K_{T4} < 0.3$  GeV/c,  $r_4(Q_4)$  decreases with decreasing temperature for lower particle number. However, the results for the high particle numbers are almost independent of temperature. In the high average-transverse-momentum region  $K_{T4} > 0.3$  GeV/c,  $r_4(Q_4)$

is obviously enhanced at large  $Q_4$  for the low temperature  $T = 80$  MeV. This is because the chaoticity parameter of two-pion HBT correlations,  $\lambda$ , increases rapidly with increasing particle momentum at large  $Q_4$  in the EPG model.

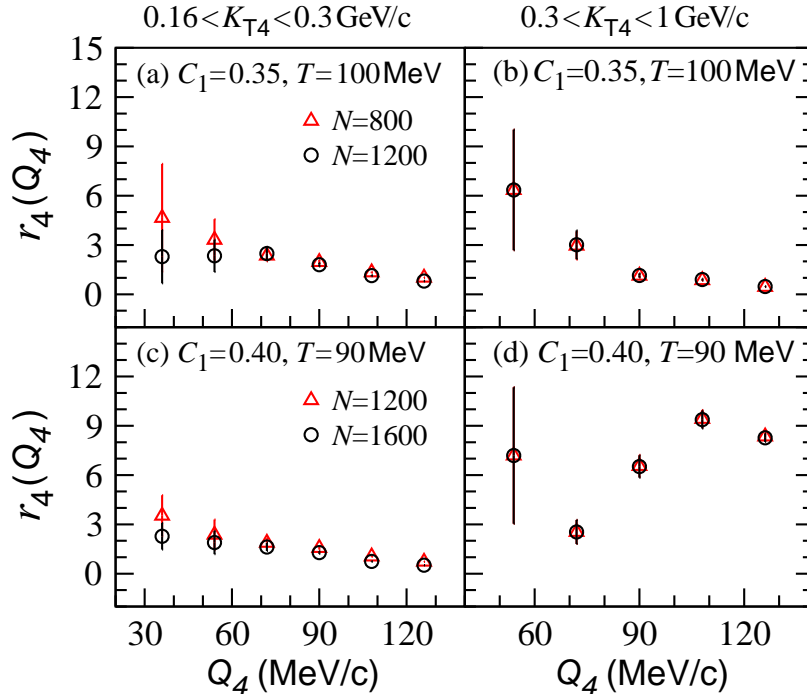


FIG. 7: (Color online) Normalized four-pion correlation functions  $r_4(Q_4)$  for the EPG sources with different particle numbers and in the transverse-momentum intervals  $0.16 < K_{T4} < 0.3$  GeV/ $c$  and  $0.3 < K_{T4} < 1$  GeV/ $c$ . The source temperature are 100 and 90 MeV when  $C_1 = 0.35$  and  $0.40$ , respectively.

In figure 7 we plot the normalized four-pion correlation function  $r_4(Q_4)$  for EPG sources in the average-transverse-momentum regions  $0.16 < K_{T4} < 0.3$  GeV/ $c$  and  $0.3 < K_{T4} < 1$  GeV/ $c$ . Here, we use the source temperatures and particle numbers as in Ref. [25] in comparing the MPC model results with the experimental Pb-Pb collision data [24]. In the low transverse-momentum region, the results of  $r_4(Q_4)$  for the large particle numbers are lower than 6 at small  $Q_4$ . This indicates that there are considerable condensations for the EPG sources with the high  $N$ . In the high transverse-momentum region,  $r_4(Q_4)$  is almost independent of particle number because of the characteristic of the EPG sources that the particles with high momenta are likely emitted from the excited states incoherently even for the source with a considerable condensation fraction. For the source with  $C_1 = 0.40$  and

$T = 90$  MeV,  $r_4(Q_4)$  is significantly enhanced at large  $Q_4$ , which reflects the two-particle correlation decreases with increasing particle momentum in the EPG model. Because the model results of  $r_3(Q_3)$  in the high transverse-momentum region almost reproduces the experimental data [24], we hope the enhancement of  $r_4(Q_4)$  in this transverse-momentum region will be identified in future experimental data analyses.

#### IV. SUMMARY AND DISCUSSIONS

Pion multiplicity have been observed to reach several thousand in heavy-ion collisions at the LHC. This high pion multiplicity possibly causes significant system condensation and leads to a partially coherent pion-emitting source. The normalized MPC functions  $r_3(Q_3)$  and  $r_4(Q_4)$  are useful for exploring the coherence of pion-emitting sources produced in high-energy heavy-ion collisions. On the basis of our previous MPC analyses in the EPG model with Bose-Einstein condensation in relativistic heavy-ion collisions, we have investigated the normalized three- and four-pion correlation functions in different average-transverse-momentum regions of three and four particles, and studied the effects of the source temperature  $T$  and particle number  $N$  on the normalized MPC functions in the EPG model. We have found that the intercepts of the normalized MPC functions at  $Q_{3,4} = 0$  are related to the chaoticity parameter of two-pion correlation,  $\lambda$ , and sensitive to the condensation of the EPG source. The values of the normalized MPC functions in low average-transverse-momentum region decrease with decreasing  $T$  and increasing  $N$ , because the source condensation increases with decreasing  $T$  and increasing  $N$ . However, these dependences of the normalized MPC functions on the source temperature and particle number become weak in an intermediate average-transverse-momentum region, which reflects the important characteristic of the EPG source that the particles with high momenta are likely emitted from the excited states incoherently even for the source with a considerable condensation fraction. In high average-transverse-momentum region, the normalized MPC functions for low source temperatures are enhanced at larger relative momenta because of the rapid increase of the two-pion chaoticity parameter  $\lambda$  with increasing particle momentum in the EPG model.

Finally, let us make an estimation of the average phase-space density  $\langle f \rangle_p$  for the EPG sources with different values of  $C_1$  parameter, particle number  $N$ , and source temperature  $T$ . Based on the method proposed by G. F. Bertsch [32], the phase-space density can be

estimated with single-particle momentum distribution and two-particle HBT radius. In the EPG model, it is assumed that the relaxation time of the system is smaller than the source evolution time and the expansion of the pion gas may approximately deal with a quasi-static process [25, 26]. Therefore, at each time during the source evolution, there is a certain system temperature  $T$  (see the Fig. 1 in Ref. [26]), and the corresponding single-pion momentum distribution is  $(d^3N/d^3p)(T) = G^{(1)}(\mathbf{p}, \mathbf{p})$  [25, 26, 28]. Using the parameterized two-pion correlation function,  $1 + \lambda \exp(-q^2 R_{\text{HBT}}^2)$ , for the spherical EPG sources, the average phase-space density is given by [32],  $\langle f \rangle_p = (d^3N/d^3p) \lambda \sqrt{\pi} / (4R_{\text{HBT}}^3)$ . We can calculate  $(d^3N/d^3p)(T)$ ,  $\lambda(p, T)$ , and  $R_{\text{HBT}}(p, T)$  [25, 26, 28] for the EPG sources, and obtain  $\langle f \rangle_{p=100\text{MeV}/c} = 1.509$  and  $\langle f \rangle_{p=500\text{MeV}/c} = 0.006$  for the parameter set ( $C_1 = 0.40$ ,  $N = 1200$ , and  $T = 100$  MeV/c). The average phase-space density decreases greatly with increasing particle momentum. The high  $\langle f \rangle_p$  at small particle momentum corresponds to a condensation. The average phase-space density at the average momentum,  $\langle f \rangle_{\langle p \rangle}$ , for the low and high source temperatures  $T = 100$  and  $150$  MeV are  $0.030$  and  $0.016$  for the parameter set ( $C_1 = 0.40$  and  $N = 1200$ );  $0.060$  and  $0.022$  for the parameter set ( $C_1 = 0.40$  and  $N = 1600$ ); and  $0.108$  and  $0.028$  for the parameter set ( $C_1 = 0.35$  and  $N = 1200$ ). The average phase-space density decreases with increasing temperature and decreasing particle number. The values of  $\langle f \rangle_{\langle p \rangle}$  for the smaller source-size parameter  $C_1 = 0.35$  are higher than those for the larger source-size parameter  $C_1 = 0.40$ .

In relativistic heavy-ion collisions, coherent emission may arise from the formation of a disoriented chiral condensate (DCC) [33–35], pionic or gluonic Bose-Einstein condensations [25–28, 36], or multiple coherent sources from pulsed radiation [37]. Our previous investigations [25] indicate that the EPG model with pion condensation can approximately reproduce the MPCs in Pb-Pb collisions at the LHC [24]. In this study, we found that the EPG model gives intercepts of the normalized MPC functions in agreement with the experimental Pb-Pb collision data [22]. The function  $r_3(Q_3)$  in the EPG model also approximately reproduces the experimental data in the high average-transverse-momentum region [22]. These EPG-model results indicate that the simple spherical EPG model may catch hold of some main characteristics of the pion-emitting sources and the system produced in heavy-ion collisions at the LHC may have a considerable condensation. As a result of the EPG model, we hope the significant enhancement of the normalized four-pion correlation function  $r_4(Q_4)$  at large relative momentum will be identified experimentally in future. On

the other hand, viscous hydrodynamics has widely been used to describe the system evolution in relativistic heavy-ion collisions. It will be of interest to develop a model of identical pion-emitting source that evolves with viscous hydrodynamics.

### Acknowledgments

This research was supported by the National Natural Science Foundation of China under Grant Nos. 11675034 and 11275037, and the China Scholarship Council. Mark Kurban, M. Sc., from Liwen Bianji, Edanz Editing China ([www.liwenbianji.cn/ac](http://www.liwenbianji.cn/ac)), edited a draft of this manuscript.

- 
- [1] M. Gyulassy, S. K. Kauffmann, and Lance W. Wilson, *Phys. Rev. C* **20**, 2267 (1979).
  - [2] C. Y. Wong, *Introduction to High-Energy Heavy-Ion Collisions* (World Scientific, Singapore, 1994), Chap. 17.
  - [3] U. A. Wienemann and U. Heinz, *Phys. Rep.* **319**, 145 (1999).
  - [4] R. M. Weiner, *Phys. Rep.* **327**, 249 (2000).
  - [5] T. Csörgő, *Heavy Ion Physics* **15** (2002) 1; arXiv:hep-ph/0001233.
  - [6] M. A. Lisa, S. Pratt, R. Soltz, and U. Wiedemann, *Annu. Rev. Nucl. Part. Sci.* **55**, 357 (2005).
  - [7] S. Pratt, *Phys. Lett. B* **301** (1993) 159.
  - [8] T. Csörgő and J. Zimányi, *Phys. Rev. Lett.* **80** (1998) 916; J. Zimányi and T. Csörgő, *Heavy Ion Physics* **9** (1999) 241; arXiv:hep-ph/9705432.
  - [9] Y. M. Liu, D. Beavis, S. Y. Chu, S. Y. Fung, D. Keane, G. VanDalen, and M. Vient, *Phys. Rev. C* **34** (1986) 1667.
  - [10] W. A. Zajc, *Phys. Rev.* **D35**, (1987) 3396.
  - [11] M. Biyajima, A. Bartl, T. Mizoguchi, N. Suzuki and O. Terazawa, *Prog. Theor. Phys.* **84** (1990) 931.
  - [12] I. V. Andreev, M. Plümer, R. M. Weiner, *Phys. Rev. Lett.* **67**, (1991) 3475;  
I. V. Andreev, M. Plümer, R. M. Weiner, *Int. J. Mod. Phys.* **A8**, (1993) 4577.
  - [13] W. N. Zhang, Y. M. Liu, S. Wang *et al.*, *Phys. Rev.* **C47**, (1993) 795;  
W. N. Zhang, Y. M. Liu, L. Huo *et al.*, *Phys. Rev.* **C51**, (1995) 922;



- W. N. Zhang, L. Huo, X. J. Chen *et al.*, Phys. Rev. **C58**, (1998) 2311;  
W. N. Zhang, G. X. Tang, X. J. Chen *et al.*, Phys. Rev. **C62**, (2000) 044903.
- [14] W. Q. Chao, C. S. Gao, and Q. H. Zhang, J. Phys. **G21**, (1995) 847;  
Q. H. Zhang, W. Q. Chao, and C. S. Gao, Phys. Rev. **C52**, (1995) 2064.
- [15] U. Heinz and Q. H. Zhang, Phys. Rev. C **56** (1997) 426;  
U. Heinz and A. Sugarbaker, Phys. Rev. C **70** (2004) 054908.
- [16] H. Nakamura and R. Seki, Phys. Rev. **C60**, (1999) 064904;  
H. Nakamura and R. Seki, Phys. Rev. **C61**, (2000) 054905.
- [17] H. Bøggild et al. (NA44 Collaboration), Phys. Lett. B **455** (1999) 77;  
I. G. Bearden et al. (NA44 Collaboration), Phys. Lett. B **517** (2001) 25.
- [18] M. M. Aggarwa et al. (WA98 Collaboration), Phys. Rev. Lett. **85** (2000) 2895;  
M. M. Aggarwa et al. (WA98 Collaboration), Phys. Rev. C **67** (2003) 014906.
- [19] J. Adams et al. (STAR Collaboration), Phys. Rev. Lett. **91** (2003) 262301.
- [20] M. Csanáda for the PHENIX Collaboration, Nucl. Phys. A **774** (2006) 611.
- [21] K. Morita, S. Muroya, and H. Nakamura, Prog. Theor. Phys. **116** (2006) 329.
- [22] B. Abelev et al. (ALICE Collaboration), Phys. Rev. C **89** (2014) 024911.
- [23] D. Gangadharan, Phys. Rev. C **92** (2015) 014902.
- [24] J. Adam et al. (ALICE Collaboration), Phys. Rev. C **93** (2016) 054908.
- [25] G. Bary, P. Ru, W. N. Zhang, J. Phys. G **45** (2018) 061502.
- [26] J. Liu, P. Ru, W. N. Zhang, C. Y. Wong, J. Phys. G **41** (2014) 125101.
- [27] V. Begun, W. Florkowski, and M. Rybczynski, Phys. Rev. C **90** (2014) 014906;  
V. Begun and W. Florkowski, Phys. Rev. C **91** (2015) 054909.
- [28] C. Y. Wong and W. N. Zhang, Phys. Rev. C **76** (2007) 034905.
- [29] M. H. Anderson, J. R. Ensher, M. R. Matthews, C. E. Wieman and E. A. Cornell, Science **269**, 198 (1995).
- [30] M. Naraschewski and R. J. Glauber, Phys. Rev. A **59** (1999) 4595.
- [31] G. J. Viana, A. Perrin, M. Schellekens, D. Boiron, C. I. Westbrook, and M. Belsley, Phys. Rev. A **74** (2006) 053607.
- [32] G. F. Bertsch, Phys. Rev. Lett. **72** (1994) 2349; Erratum, Phys. Rev. Lett. **77** (1996) 789.
- [33] C. Greiner, C. Gong, and B. Muller, Phys. Lett. B **316** (1993) 226.
- [34] J. Bjorken, Acta Phys. Pol. B **28** (1997) 2773.

- [35] K. Rajagopal, arXiv:hep-ph/9703258.
- [36] J. P. Blaizot, F. Gelis, J. F. Liao, L. McLerran, and R. Venugopalan, Nucl. Phys. A **873** (2012) 68.
- [37] E. Ikonen, Phys. Rev. C **78** (2008) 051901.